Nanoclustering of hydrogen in ion-implanted and plasma-grown amorphous silicon

S. Acco
Debye Institute, Utrecht University, P.O. Box 80000, 3508 TA Utrecht, The Netherlands

D. L. Williamson
Department of Physics, Colorado School of Mines, Golden, Colorado 80401

W. G. J. H. M. van Sark,* W. C. Sinke,† and W. F. van der Weg
Debye Institute, Utrecht University, P.O. Box 80000, 3508 TA Utrecht, The Netherlands

A. Polman
FOM Institute for Atomic and Molecular Physics, Kruislaan 407, 1098 SJ Amsterdam, The Netherlands

S. Roorda
Group de Recherche en Physique et Technologie des Couches Minces, Département de Physique, Université de Montréal, Case Postale 6128 succursale centre-ville, Montréal, Canada QC H3C

(Received 28 January 1998)

We report a systematic study of small-angle x-ray scattering and Raman spectroscopy on hydrogen-implanted amorphous silicon (a-Si) and standard device-quality plasma-grown a-Si:H, both having a hydrogen concentration of 11 at. %. The modifications of short-range and medium-range structural order induced by annealing are investigated. We find that annealing causes the formation and growth of nanoscale H complexes in both materials. However, the volume content of the H nanoclusters is strongly influenced by the disorder in the original structure, remaining smaller by a factor of 3 in the a-Si:H with respect to the H-implanted sample. We discuss qualitative resemblances and quantitative differences of the structural evolution of H-implanted a-Si and a-Si:H in terms of H solubility and defect structure in a-Si. In addition, the study of a-Si implanted with H at different concentrations shows that the amount of H nanoclustering increases superlinearly with the concentration of H atoms exceeding solubility.
[S0163-1829(98)00843-1]

I. INTRODUCTION

A vast number of experimental investigations of hydrogenated amorphous silicon (a-Si:H) has revealed a high complexity of the hydrogen microstructure in this material. Various covalent bondings of H to Si have been recognized by infrared-absorption spectroscopy (IR), the dominant ones being $\equiv$Si—H and $(=\text{Si}=\text{H}_2)_n$, $n \geqslant 1$.[1] In addition, nuclear magnetic resonance[2,3] has identified two distinct local environments for H. According to these measurements, hydrogen is present in an isolated phase (i.e., the mean spacing between H atoms is larger than 5–8 Å) and in a clustered phase. In device-quality material, clusters contain 5–7 H atoms, the configurations of which are not clearly recognized. Finally, the morphology of the grown films is generally characterized by the presence of low-density defects (voids or H-rich regions) on the nanometer scale.[4–6] The increase of the H content in the films to values higher than 10–15 at. % is usually accompanied by an increase of the amount of H present in the clustered phase and of nanoscale inhomogeneities.[3,7,8]

These results have raised the question whether only a definite amount of hydrogen is beneficial to a specific amorphous structure, that is, in the passivation of electronic defects and in the release of the network strain.[9] Hydrogen incorporation into the network above that definite concentration would then lead solely to an increase of the H in the clustered phase,[10] a configuration believed to be more loosely bound to Si than the isolated phase. Posing the question in other words, it may be that either the H atoms added above those ''beneficial'' are just less effective in the defect passivation, or they are responsible for the creation of additional structural and/or electronic defects. There have been several efforts towards the understanding of the influence of the variation of H concentration on the structural properties, mostly by investigating the effects of post-hydrogenation in plasma-grown a-Si:H.[11–13] It seems, however, very difficult to draw general conclusions, mainly because the structural properties of a-Si:H depend strongly on the plasma conditions and substrate temperature during growth. Therefore, the structural properties and the H concentration cannot be varied independently.

This question seems to have an answer in the case of amorphous silicon prepared by ion implantation. Ion-implanted pure a-Si (unhydrogenated) appears to be attractive as a model system since it is void-free[14] and its structural properties are reproducible.[15,16] As-implanted pure a-Si exhibits a density of defects of the order of 1 at. %,[15,16] of which only a small fraction (~0.04 at. %) consists of paramagnetic defect centers, i.e., dangling bonds.[17] Introducing H into this system, again by ion implantation, represents a well-controlled method to vary the H concentration indepen-

 ©1998 The American Physical Society

dently of other parameters.[18,19] Previous experiments on H-implanted amorphized Si (Refs. 20 and 21) have indicated that the alloy has a stable network structure only when containing H below and up to 3–4 at. %. Hydrogen-rich defects on the nanoscale are observed to nucleate upon annealing when the H content exceeds this concentration, which defines the solubility limit of H in amorphized Si. In other words, results[20] have suggested a finite concentration of H atoms that can be accommodated in the Si network sites and that move upon annealing while remaining dissolved as Si-H bonds in the alloy phase.

Given the large knowledge base regarding the structure of amorphized materials, another interesting question is whether and how the defect density of 1–2 at. % present in the amorphous structure before hydrogenation[15,16] can be related to the H solubility of 3–4 at. %.[20] Unfortunately, we encounter here an unresolved problem: the defect structure before and after hydrogenation can never be directly compared, for the introduction of H itself modifies the network. Relaxation and defect-annealing processes occur concomitant with H motion. These processes involve modifications of the atomic configurations and the creation of metastable defects.[22,23]

To deepen our knowledge on the influence of the network disorder on the H clustering process, we have thus adopted a different approach. A comparative study is undertaken between the amorphized material, characterized by a high disorder[24] and defect density,[16,17] and device-quality, plasma-grown *a*-Si:H. The initial H content is similar in the differently prepared samples. We have used small-angle x-ray scattering (SAXS) and Raman scattering to obtain complementary information on the atomic and nanoscale disorder of the alloy structure. In this paper, it is demonstrated that, for deposited *a*-Si:H, annealing of an initially homogeneous structure on the nanometer scale leads to a process of H clustering, followed by a precipitation on a larger scale, similar to that of H-implanted *a*-Si containing H in excess of the solubility limit. In addition, it is observed that the degree of H clustering in plasma-grown *a*-Si:H is much lower than that shown by the implanted samples. The influence of structural properties, such as the initial H content, the defect state, the preparation temperature, and the presence of H-related defects, on the amount of H nanoclustering are discussed.

II. EXPERIMENT

A. Samples

H-implanted samples

For SAXS measurements a 75-μm-thick double-polished Si wafer was irradiated with Si ions at various ionization states and energies ranging from 0.5 to 17 MeV. The bombardment produced an amorphous layer of 8.5 μm thickness. The amorphized layer was then irradiated with H_2 ions at 19 energies ranging from 50 to 500 keV/amu. The total injected dose was 3.16×10^{18} cm^{-2}. All implants were carried out on a liquid-nitrogen-cooled target. Figure 1 illustrates the hydrogen depth profile for the H-implanted sample in the as-implanted state, as measured by secondary-ion mass spectrometry (SIMS). The profile exhibits 19 peaks, of maximal concentration of 12$\pm$1 at. %, corresponding to the different

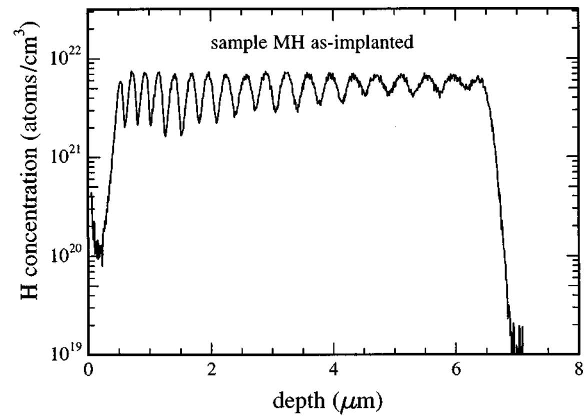

FIG. 1. The hydrogen SIMS depth profile for the as-implanted MH sample.

implantation energies. SAXS and SIMS measurements were performed on the same sample.

Implanted samples will be referred as to the MH [or *a*-Si(H)] samples. MH indicates a *medium* H content that falls in between that of the low H and HH (high H) samples previously studied.[20,25]

Glow-discharge deposited samples

Device-quality intrinsic *a*-Si:H films were produced using plasma-enhanced chemical vapor deposition (PECVD). A mixture of SiH_4 and H_2 at the ratio 1:1 with a pressure of 0.35 mbar was used during deposition. Films deposited under the same conditions were used as the intrinsic layer to make a single-junction solar cell with a 10% initial efficiency.[26]

High-purity aluminum foil and standard crystal Si wafers were used as substrates for SAXS and Raman spectroscopy, respectively. The substrate temperature during deposition was 250 °C. Elastic recoil detection (ERD) measurements were made in the sample on *c*-Si in the as-deposited state and after annealing at 425 °C for 1 h (not shown). The sample exhibits an initially flat H distribution of 11 at. %.

The mass density of the film deposited on Al foil was determined by flotation analysis to be 2.23 g/cm^3. These films will be referred to as the GD samples.

Thermal treatments

Ion-implanted and deposited layers were subjected to subsequent anneals up to 4 h at temperatures ranging from 200 to 500 °C, in 50 °C increments up to 400 °C and in 25 °C increments for higher temperatures.

B. Measurements

Raman scattering

Raman measurements were performed with the 514.5-nm line of a Ar-ion laser. At this wavelength, the penetration depth is ~60 nm in *a*-Si:H. To avoid laser-induced annealing or crystallization of the probed layer, the beam was defocused and the power of the laser was kept below 40 W/cm^2. The width of the transverse-optic-like (TO) peak of the Stokes spectra was estimated by fitting the spectra with a sum of Gaussian functions corresponding to the different

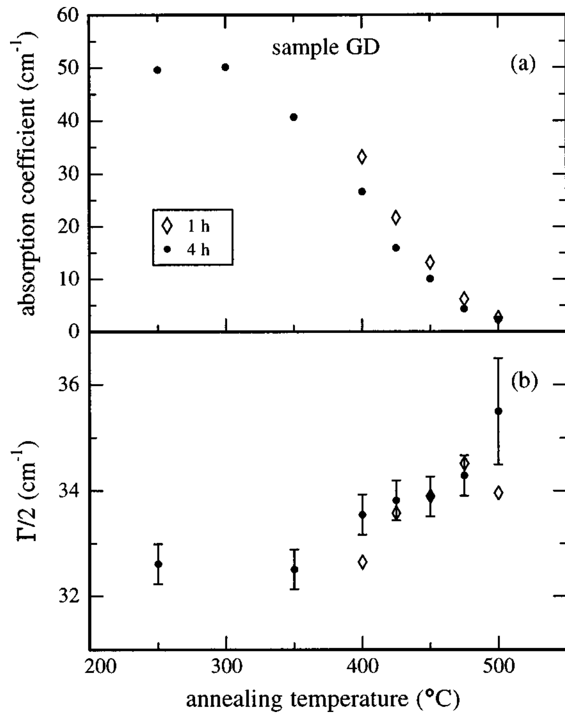

FIG. 2. The integrated absorption coefficient of the stretching modes of the GD sample (a) and the half-width at half maximum (Γ/2) of the Raman TO peak (b) as a function of the annealing temperature.

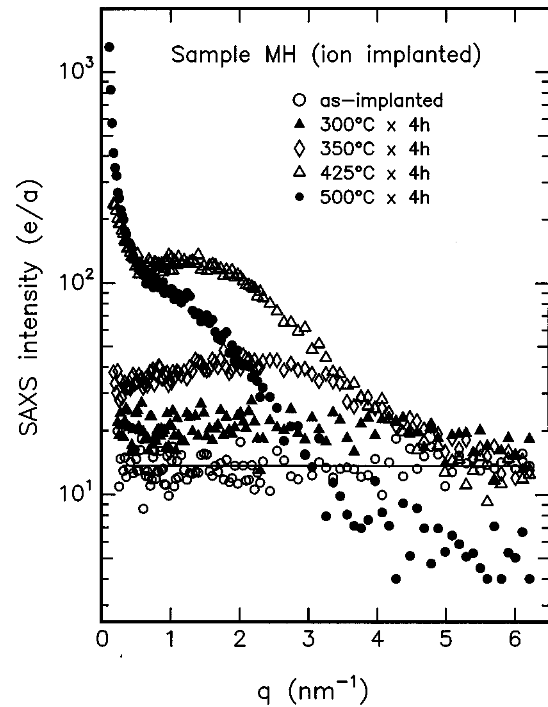

FIG. 3. SAXS intensities from the H-implanted a-Si MH sample in the as-implanted state and after subsequent annealing for 4 h at various temperatures. The line through the data of the as-implanted sample is drawn to guide the eye.

spectral bands that characterize the a-Si. For each experiment run, a spectrum of a standard sample (pure a-Si) was taken and the linewidth of the TO peak estimated by fitting. The standard deviation of the measured and fitted values of the linewidth for the standard a-Si sample should then account for the error both in the experiment and in the fitting procedure used for the data analysis.

Small-angle x-ray scattering (SAXS)

The SAXS experiments were performed in a Kratky camera with a line-collimated setup. The radiation source was a Rigaku rotating anode (Cu) x-ray generator; the Cu $K\alpha$ radiation ($\lambda = 1.54$ Å) was selected with a crystal monochromator. The count rate was recorded by a proportional counter as a function of the momentum transfer $q = (4\pi/\lambda)\sin\theta$ (2θ is the scattering angle) from about 0.1–6 nm^{-1}. Further experimental details are given in Ref. 6.

III. RESULTS

A. Raman spectroscopy

The half width at half maximum Γ/2 of the TO peak observed in the Raman spectra of a-Si provides information on the short-range structural disorder of the amorphous network.[27]

Figure 2 shows the changes in Γ/2 as a function of the annealing temperature in correlation with the variation of the integrated absorption coefficient for the IR absorption stretching band in the a-Si:H sample. Details on the IR measurements are reported elsewhere,[28] but it is worth noting that (1) a very good agreement exists between the H content evaluated by ERD and that from the integrated absorption coefficient;[29] (2) H atoms are bonded to Si mostly as monohydrides. The data shown in Fig. 2(a) indicate that the loss of bonded H starts at annealing temperatures higher than 300 °C.

The value of Γ/2 in the as-deposited state is 32.5 ± 0.5 cm^{-1} [Fig. 2(b)], which corresponds to a value of $\sim 8°$ for the $\Delta\vartheta$ (the root-mean square bond-angle distortion).[24] The position of the TO-like peak is at 478 ± 2 cm^{-1}. Annealing at temperatures up to 400 °C induces no changes in Γ/2, outside the experimental uncertainty. After annealing at 400 °C for 4 h and at higher temperatures, a significant increase in Γ/2 is observed.

The sample surface of the annealed GD sample was examined by optical microscope and after thermal treatment at 500 °C appeared to be covered with microcracks, which caused a strong light scattering from the incident laser beam. This affected the Raman spectra and the error associated with the value for the 500 °C-annealed sample (4 h) is the mean-square deviation of the measurements on several distinct positions of the sample surface. No crystalline phase was detectable after the last annealing.

B. SAXS results

1. H-implanted a-Si

Figure 3 summarizes SAXS data from the MH sample. The scattering intensity for the sample in the as-implanted state and after annealing up to and including 250 °C (not shown) is essentially independent of the momentum transfer q. It follows that (1) the signal contains only diffuse SAXS intensity, which originates from atomic-scale density fluctuations; (2) nanoscale inhomogeneities, if present, are well be-

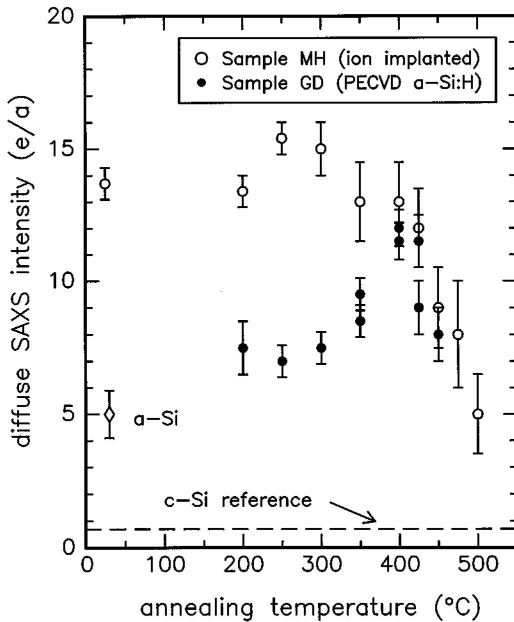

FIG. 4. SAXS diffuse intensity for the samples MH and GD in the initial state and after subsequent annealing at various temperatures. Annealing times were 4 h for the MH sample and from 1 to 4 h for the GD sample. We show also the value of the diffuse SAXS for the as-implanted pure a-Si from Ref. 14 and for c-Si.

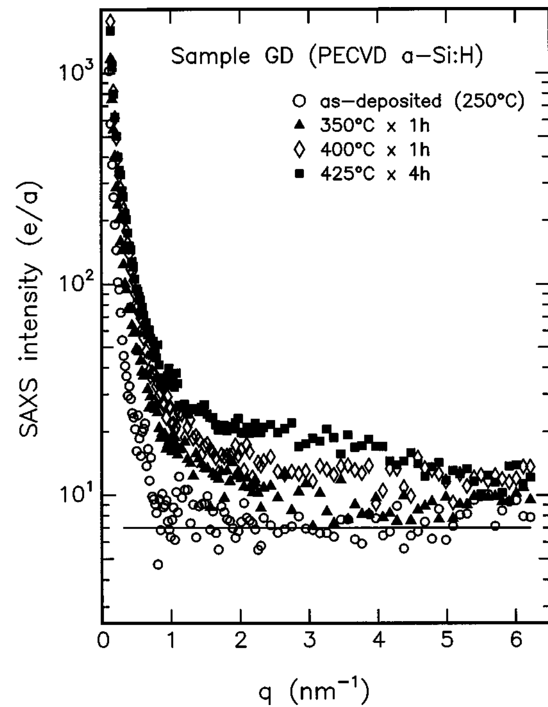

FIG. 5. SAXS intensities from the a-Si:H GD sample in the as-deposited state and after subsequent annealing at various temperatures. The line through the data of the as-deposited sample is drawn to guide the eye.

low the present SAXS sensitivity of 0.1 vol %.[6] In order to examine the variation in the diffuse scattering intensity upon annealing, the data of each scan were averaged in the $1.5 \leqslant q \leqslant 6\ \mathrm{nm}^{-1}$ range. Results are reported in Fig. 4. For comparison, the diffuse intensities originating from amorphized pure a-Si (no H),[14] and from the c-Si reference are also shown. Annealing at 200 °C does not cause any detectable change in the SAXS diffuse intensity of the MH sample, while an increase is evident after annealing at 250 °C.

As a result of annealing at 300 °C, the scattering intensity increases and exhibits a weak q dependence (Fig. 3), consistent with the presence of 0.11–0.15 vol % of low-density nanoscale structural defects of 0.5 ± 0.05 nm average radius. Heating above 300 °C induces a systematic increase in the SAXS signal, which demonstrates an increase of the volume content of the inhomogeneities. The presence of a relative maximum in the intensity at $q \geqslant 1\ \mathrm{nm}^{-1}$ indicates the occurrence of interference effects between the particles (in this contest an inhomogeneity is treated as a single ''particle''). This implies that the interparticle distance is of the same order as the particle size and that particles are correlated in position. The shift of the maximum with annealing temperature toward lower q is representative of a larger separation of the inhomogeneities. The steeper rate of fall-off of the intensity versus q with higher anneal temperatures demonstrates growth of the particles. After annealing at 500 °C, the average radius of the inhomogeneities has increased to a value of 1.1 ± 0.1 nm. At this temperature regime, no interparticle interference is detected in the data.

The increase of the SAXS signal upon annealing at $T > 300\ °C$ occurs in concomitance with the reduction of the diffuse scattering component, observable in the large-q portion of the data in Fig. 3. This agrees with a H loss from the matrix or a reduction of the alloy clustering, which causes a decrease of the Laue monotonic scattering (Sec. IV B). Values of the diffuse component at high-annealing temperatures in Fig. 4 have a relatively large uncertainty because they are an average of the few high-q data points less affected by the q-dependent contribution.

A relatively high density of microcracks and blisters on the micrometer scale was observed by optical microscope on the surface of the MH sample after annealing at $T = 500\ °\mathrm{C}$. It is likely that these surface defects are related to the enhanced scattering at very low-q values observed in the SAXS intensity for the MH sample annealed at temperatures higher than 350 °C. The low-q signal denotes the presence of density fluctuations on a much larger scale. The contribution of this smaller-angle intensity to the signal increases with annealing temperature.

2. PECVD a-Si:H (GD sample)

SAXS intensities from the GD sample in the as-deposited state and after various thermal treatments are presented in Fig. 5. As a general observation, all the signals exhibit a strong rise at smaller angles ($q \leqslant 1\ \mathrm{nm}^{-1}$), indicative again of larger-scale objects ($\geqslant 10$ nm). A low-q signal is usually observed on a-Si:H and will be discussed more in detail in Sec. IV C. We focus the attention here on the portion of the data of $q \geqslant 1\ \mathrm{nm}^{-1}$. A very low scattering intensity with essentially no q dependence characterizes the signal of the deposited film in the initial state ($T_s = 250\ °\mathrm{C}$). Annealing at temperatures up to the deposition temperature does not produce any change in the SAXS intensity, and the little variation observed in the 300 °C-annealed sample (not shown) is not considered to be significant. Results indicate once again that the signal consists of only diffuse scattering intensity

and therefore that nanometer-scale inhomogeneities are below the technique sensitivity in this temperature regime. Similar to the implanted sample, averages of the SAXS data in the 1.5–6 nm^{-1} q range were calculated and are compared with those of the MH sample in Fig. 4.

Thermal treatments at temperatures higher than 300 °C modify the structure of the film. The diffuse scattering systematically increases after annealing up to and including 400 °C, and is followed by a decrease at higher temperatures (Fig. 4). After annealing above 350 °C, a q dependence is clearly visible in the SAXS signal (Fig. 5). Data associated with the sample annealed at 400 °C for 4 h are consistent with 0.10–0.13 vol. % of inhomogeneities of 1.2 ± 0.3 nm average radius. The volume content of these nanoscale particles increases following annealing at higher temperatures, whereas their average radius appears to decrease.

To inspect the shape of the particles, the 425 °C-annealed sample was tilted at 45° relative to the beam direction. No difference in the SAXS signal was detected with respect to the nontilted data (not shown), suggesting that the inhomogeneities have either spherical symmetry or are randomly oriented.

After anneals higher than 350 °C, the a-Si:H sample was also measured by x-ray diffraction to check for the occurrence of the crystallization in the amorphous layer. The crystalline phase was detected after annealing at 450 °C for 4 h. It is worth noting that Raman measurements have found no evidence of the crystalline phase on the sample deposited on c-Si substrate under the same conditions, and annealed at temperatures as high as 500 °C (Sec. III A). The relatively low-temperature crystallization of the a-Si:H film deposited on aluminum was previously observed[30] and attributed to the rapid interdiffusion of Si and Al with consequent enhancement of the crystallization process.

3. Dependence of the inhomogeneity content on the annealing temperature

Figure 6 illustrates the variation of the volume fraction and of the average radius of the nanoscale particles as a function of the annealing temperature for the MH and the GD samples. Values result from the analysis of the SAXS data, which is described in the following section. Data are compared with results from a previously studied implanted sample containing 20 at. % H (HH sample).[20] The different preparation conditions of the samples discussed in this work are summarized in Table I.

The volume fraction f_2 of the nanoscale inhomogeneities of the GD sample remains lower than that of the implanted material at any temperature regime [Fig. 6(a)]. Besides, the annealing temperature at which the nanoparticles are detected differs in the two cases. Nanoparticles appear in the implanted material above 250 °C, whereas temperatures above 350 °C are necessary for the GD sample.

We turn now to the comparison between the MH and the HH samples, implanted with hydrogen at concentrations of 12 and 20 at. %, respectively (Table I). For both samples, the average radius monotonically increases with the annealing temperature [Fig. 6(b)], from a value of 0.5 nm (the minimum size that can be presently detected by SAXS) to a value of about 1.4 nm. The volume fraction f_2 of the inhomogeneities increases likewise for the two samples at annealing temperatures up to and including 400 °C. At higher temperatures, the behavior of the two samples diverges. While for the MH sample, f_2 saturates and then decreases, the volume fraction for the HH sample keeps on increasing. After annealing at 500 °C, f_2 has increased to a value of 2.5% for the HH sample, whereas the f_2 value is 0.4% for the MH sample. At this point, it is important to note that the 20 at. % sample received a *total* injected dose similar to the MH sample ($\sim3\times10^{18}$ cm^{-2}). However, the HH sample received 10 H implants, while the presently studied sample received 19 implants (Fig. 1), over the same thickness. This implies a less uniform initial H concentration in the HH sample than in the MH sample: the distance between the H peaks in the former case is nearly twice as large. Nevertheless, a large divergence in the volume fraction for temperatures above 400 °C is found.

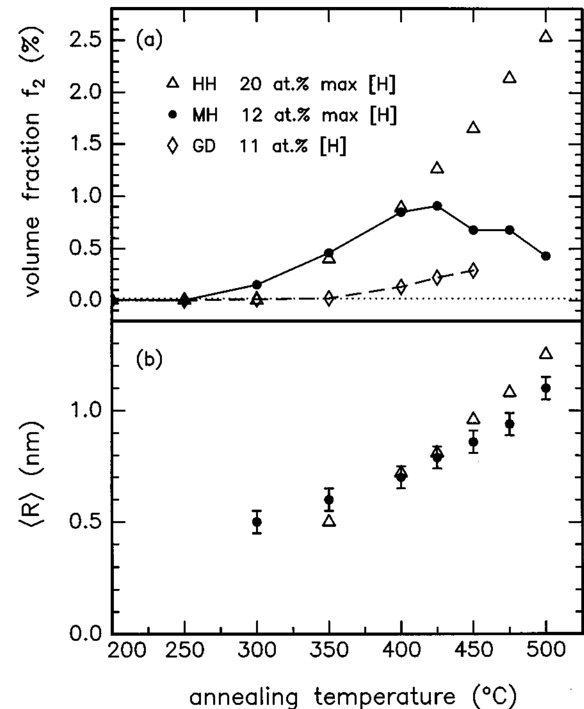

FIG. 6. (a) Volume fractions f_2 of nanoscale inhomogeneities for the H-implanted a-Si with 12 at % (MH sample) and the PECVD a-Si:H sample (GD sample), which contains 11 at % H. Also shown are the data for the HH sample with 20 at. % H peak concentration (HH sample, from Ref. 20, see Table I). Lines are drawn to guide the eye. (b) The average radius of the inhomogenities for the MH and HH samples.

IV. SAXS ANALYSIS

A. Fitting of the data

In the SAXS regime, the scattering intensity can be considered to consist of three distinct contributions,[6]

$$I(q)=I_D(q)+I_M(q)+I_P(q), \tag{1}$$

where I_D is the diffuse SAXS and I_M the scattering intensity from electron-density fluctuations on the nanometer scale. $I_P(q)$ represents the Porod term, which is significant only in

TABLE I. Summary of the preparation conditions of the samples. For the H-implanted samples, the values of [H] refer to the H-peak concentration.

Sample label	Description	[H] (at %)	Preparation
MH	Si-amorphization+H implantation	12±1	ion implantation
GD	deposited a-SiH	11±0.5	PECVD deposition
HH[a]	Si amorphization+H implantation	20±0.5	ion implantation
a-Si, as-implanted[b]	Si amorphization, as-prepared	0	ion implantation
a-Si, relaxed[b]	Si amorphization+500 °C annealing	0	ion implantation

[a]From Ref. 20.
[b]From Ref. 14.

presence of a raise of the signal in the smaller-angle region. In line-collimated geometry, $I_P(q)=A/q^3$ (A is the Porod constant).

SAXS data were analyzed according to Eq. (1). In the GD sample, only very slight evidence of an interference effect was found for the smaller particles present after annealing at $T>400\,°\mathrm{C}$. Particles were therefore treated as independent and the term $I_M(q)$ was evaluated using a theoretical intensity function that represents a spatial distribution of spherical objects of different radii.[31] Results of the fittings are reported in Table II. $\langle R\rangle$ is the average of 5–10 radii of the particles used in the fitting. The size distribution of the particles inferred from the fitting of the GD sample annealed at $T>300\,°\mathrm{C}$ indicates that there is a predominant small-size component (<1 nm) along with some small fractions of larger size. The latter, however, can have a big effect on the average size $\langle R\rangle$ of the particles reported in Table II.

For fitting the data from the MH-annealed sample, it was necessary to take into count the interparticle interference. Experimental intensities were analyzed by using the Percus-Yevick hard-sphere model.[32] The scattering intensity is given by

$$I_M(q)=CR^2S(qD)F(qR). \tag{2}$$

C is a proportionality factor to convert the intensity to electron units (electron/atom=e/a); $F(qR)$ is the scattering amplitude for a sphere of radius R, and $S(qD)$ is the pair-correlation structure factor with D the hard-sphere diameter. The radius R probably represents the average of a fairly narrow distribution. Results of the fits are reported in Table III. Since a previous investigation by transmission electron microscopy[21] demonstrated that the shape of the inhomogeneities is spherical, the assumption of an isotropic interaction, implicit in Eq. (2), is highly accurate. After annealing at 500 °C, the interference effect is not apparent in the data that were well fitted with a theoretical function for noninteracting objects (Table III).

The volume fraction f of the nanoparticles was estimated from the two-phase relation[33]

$$f(1-f)=Q_M/2\pi^2\langle\Omega\rangle(\Delta n)^2, \quad Q_M=(q_s/2)\int qI_M(q)dq, \tag{3}$$

where q_s is an experimentally determined calibration constant based on the exact slit geometry, $\langle\Omega\rangle$ is the average atomic volume of the sample, and Δn is the difference in electron density of the two phases. We have calculated the volume fraction by taking two values for the density in the particles. One value supposes that inhomogeneities are voids (i.e., zero) and the other assumes an internal pressure of 0.2 GPa. The last value was the estimated internal pressure in H_2

TABLE II. Results from SAXS analyses of the GD sample. Q is the total integrated intensity (including the Porod term), Q_M is the integrated intensity from Eq. (3), f_1 and f_2 are the volume fractions of the particles assuming zero and a high-pressure H_2 electron density, respectively. A is the Porod constant and $\langle R\rangle$ is the average radius of the particles.

Annealing state	Q ($10^{23}e$/a cm^3)	Q_M ($10^{23}e$/a cm^3)	f_1 (vol %)	f_2 (vol %)	A (e/a nm^3)	$\langle R\rangle$ (nm)
as-depos.	0.4±0.1	0	0	0	1.3±0.1	
200 °C×4 h	0.5±0.1	0	0	0	1.6±0.2	
250 °C×4 h	0.5±0.1	0	0	0	1.5±0.2	
300 °C×1 h	0.7±0.1	0.1±0.1	0.01	0.01	1.9±0.2	2. ±1
350 °C×1 h	1.2±0.1	0.5±0.1	0.03	0.04	2.7±0.3	1.4±0.4
350 °C×4 h	1.5±0.2	0.4±0.1	0.02	0.03	3.3±0.3	1.5±0.4
400 °C×1 h	2.1±0.2	0.9±0.1	0.05	0.07	3.8±0.4	1.6±0.3
400 °C×4 h	2.6±0.3	1.7±0.2	0.10	0.13	3.1±0.5	1.2±0.3
425 °C×1 h	3.3±0.3	2.3±0.2	0.13	0.18	3.3±0.5	1.0±0.2
425 °C×4 h	4.7±0.4	3.6±0.3	0.20	0.28	3.3±0.5	0.7±0.2
450 °C×4 h[a]	6.9±0.7	3.5±0.4	0.20	0.27	11. ±1	1.4±0.3

[a]After annealing at 450 °C for 4 h crystallization has started.

TABLE III. Results from SAXS analyses of the MH sample. Q_M is the integrated intensity from Eq. (3), f_1 and f_2 are the volume fractions of the particles assuming zero and a high-pressure H_2 electron density, respectively. A is the Porod constant, R is the radius of the nanoparticles (single-size), D is the effective hard-sphere diameter.

Annealing state	Q_M ($10^{23} e/a\,\mathrm{cm}^3$)	f_1 (vol %)	f_2 (vol %)	A ($e/a\,\mathrm{nm}^3$)	R (nm)	D (nm)
as-impl.	0	0	0	0		
200 °C×4 h	0	0	0	0		
250 °C×4 h	0	0	0	0		
300 °C×4 h	2.0±0.3	0.11	0.15	0	0.50±0.05	1.5±0.5
350 °C×4 h	6.0±0.3	0.34	0.46	0	0.60±0.05	2.0±0.5
400 °C×4 h	10.9±0.5	0.62	0.85	0.1±0.1	0.70±0.05	2.7±0.5
425 °C×4 h	11.7±0.5	0.66	0.91	1.8±0.2	0.79±0.05	3.2±0.5
450 °C×4 h	8.8±0.5	0.50	0.68	1.8±0.2	0.86±0.05	3.8±0.5
475 °C×4 h	8.4±0.5	0.48	0.66	1.9±0.2	0.94±0.05	4.0±0.5
500 °C×4 h	5.5±0.5	0.31	0.42	1.7±0.2	1.1±0.1	

cages for which there was evidence in a-Si:H.[34] In addition, previous results on implanted samples[20] have suggested that the formed inhomogeneities are H_2-filled bubbles. Results are listed in Tables II and III.

B. Atomic-scale fluctuations: diffuse scattering

We turn now to the diffuse-scattering component of the SAXS signal (Fig. 4). The distinct contributions that give rise to the diffuse scattering are discussed in more detail in Refs. 6 and 14. It is however worth recalling here a few notions. The diffuse intensity can be written as

$$I_D = I_C + I_{\mathrm{th}} + I_{\mathrm{sd}} + I_{\mathrm{Lm}}, \tag{4}$$

where I_C is the contribution arising from incoherent Compton scattering and I_{th} that from thermal diffuse scattering. These contributions are expected of the same order as the signal from c-Si and small if compared to the experimental values from amorphous materials, as seen in Fig. 4. I_{sd} accounts for the static-disorder scattering of the amorphous network and is the principal cause of the observed difference between the signal from pure (unrelaxed) a-Si and c-Si.[14]

Hydrogen atoms introduce atomic-scale composition fluctuations that give rise to the Laue monotonic scattering (I_{Lm}), the fourth term in Eq. (4). Under the assumption of a binary random alloy $A_{1-x}B_x$, I_{Lm} can be expressed in electron units by[35]

$$I_{\mathrm{Lm}} = x_A(1-x_A)(Z_A - Z_B)^2\left[1 - \frac{1-\Omega_B/\Omega_A}{\gamma}\right]^2, \tag{5}$$

where Z_A and Z_B are the atomic numbers of the relative elements. The factor in the square brackets takes into count the difference in atomic volume between the elements A and B and γ is a constant that includes the Poisson ratio, taken as 1.23 for c-Si. For H in Si, $\Omega_H/\Omega_{\mathrm{Si}} \sim 0.4-0.5$.[18,36]

A presence of a random distribution of vacancies in Si will also contribute to the Laue scattering, according to Eq. (5). If c is the atomic fraction of vacancies, Eq. (5) becomes

$$I_{\mathrm{Lm}} = cZ^2\left[1 - \frac{1-\Omega_{\mathrm{vac}}/\Omega_{\mathrm{Si}}}{\gamma}\right]^2, \tag{6}$$

where Z is the atomic number of Si and $\Omega_{\mathrm{vac}}/\Omega_{\mathrm{Si}} \sim 1/3$.[37]

Deviations from Eq. (5) may provide information on the short-range H clustering, for instance, the presence of polyhydride configurations or monohydride-clustered groups, rather than a random-spatial distribution of single H atoms. The same argument holds for short-range vacancy defects. This point will become important in the interpretation of the results described in Sec. V.

C. Scattering in the smaller-angle region ($q \leqslant 1\ \mathrm{nm}^{-1}$)

A significant SAXS signal at $q \leqslant 1\ \mathrm{nm}^{-1}$ has been generally observed on deposited a-Si:H films and on related alloys, regardless of the morphology of the films.[4–6,8,38] A dependence of the smaller-angle scattering intensity on the quality of the films was nonetheless detected, and low-quality samples often exhibit a large Porod term, which extends to higher q values. Since a-Si:H samples measured by SAXS are commonly deposited on Al foils, we consider the roughness of the substrate surface, and thus of the film, as a possible source of this signal. In fact, experimental data on a-Ge:H (Ref. 39) have shown a strong Porod signal from films on Al foil, which reduces dramatically for layers grown on c-Si. These results suggest that the surface roughness contributes to the smaller-angle signal.

The presence of large-scale (>10 nm) low-density structural features in the bulk should also be considered. Only a very small density of larger-scale features is required to give rise to the observed Porod term. Assuming voids of similar shape and size, one can show that the Porod constant is given by[33]

$$A = q_s^{-1} f \Omega (\Delta n)^2 \pi^2 S/V, \tag{7}$$

where S/V is the surface to volume ratio of the void. For spherical voids, $S/V = 3/R$, and values of A from 1 to $10\ e/a\ \mathrm{nm}^{-3}$ (Table II) can be produced by $f = 0.03-0.3$ vol % of voids of 20-nm radius. If these larger-scale features are not true voids, but H-rich regions,[4] then Δn will be smaller and f correspondingly larger. Since a Porod term is generally observed, this hypothesis would im-

ply the systematic presence of a residual columnar morphology also in device-quality deposited a-Si:H.[6]

The analysis of the ion-implanted material can significantly contribute to the understanding of this issue. SAXS samples prepared by ion implantation consist of an amorphous layer on c-Si substrate, which is characterized by a very low-scattering intensity (Fig. 4). Previous measurements showed that SAXS signals from H-implanted a-Si (Ref. 20) and pure a-Si (Ref. 14) exhibit a low-q enhancement *only* in the presence of surface defects, independent of the bulk properties of the layers. The SAXS of the MH sample reveals the presence of larger-scale objects after annealing at relatively low temperatures (Table III). Indeed, surface microcracks and blisters are visible on the sample surface after annealing at $T=500\,^{\circ}\mathrm{C}$ (Sec. III B). Such defects were perhaps already present after lower-temperature anneals. After relatively high-temperature annealing, when the diffusion coefficient of H is high, larger H_2-bubbles are expected to accumulate at the a-Si(H)/c-Si interface, contributing to the low-q signal. Finally, it is to be noted that the Porod term remains much smaller in the MH sample than in the GD sample, for any annealing temperature (Tables II and III).

V. DISCUSSION

A. Initial state: structural disorder and hydrogen-related defects

No nanostructure is detected in the SAXS intensities for either the MH or the GD sample in the as-prepared state (Figs. 3 and 5). In the case of the MH sample, this result is not surprising since previous studies have indicated that H implantation without annealing does not induce nanovoids, even to a peak fluence of 20 at. %.[20] The low SAXS signal that characterizes the GD sample is comparable with those recently measured on a few device-quality hot-wire and plasma-grown a-Si:H films,[6] which also exhibited volume fractions of low-density defects below the present SAXS detection limit.

In addition to the homogeneity of the nanostructure, IR spectra[28] show that both samples contain H atoms, which are bound to Si predominantly as monohydrides. Yet, large differences in the atomic-scale disorder state are observed in the two materials.

Ion-implanted a-Si is characterized by a high degree of structural disorder. Earlier Raman-scattering studies have reported the value of $\sim 44\ \mathrm{cm}^{-1}$ for $\Gamma/2$ ($\Delta\vartheta \sim 12°$) in pure a-Si made by ion implantation[24] and in high-dose ion-irradiated a-Si:H.[40] On the basis of these results it was concluded that ion irradiation produces atomic displacements and damage (thus, structural disorder), independent of the presence of H, at least in the as-prepared state. The bond-angle distortion in the MH sample is therefore expected to be of the same order as that of pure a-Si, because the introduction of hydrogen occurred by implantation.

Raman scattering yielded $32.5 \pm 0.5\ \mathrm{cm}^{-1}$ for $\Gamma/2$ ($\Delta\vartheta \sim 8°$) in the GD sample [Fig. 2(b)], much lower than the values from the irradiated materials.[24,40] Earlier systematic investigations[40] on differently prepared a-Si:H (hot-wire and glow-discharge films with various H contents) found $\sim 33\ \mathrm{cm}^{-1}$ as the lowest value for $\Gamma/2$. This value, like the one measured in the GD sample, was associated with the minimum structural disorder possible in a-Si:H. We note in passing that the absence of a decrease of $\Gamma/2$ upon annealing at $T \leqslant 350\,^{\circ}\mathrm{C}$ [Fig. 2(b)] of the GD sample is in distinct contrast with a decrease in $\Gamma/2$, generally observed in irradiated a-Si and more disordered a-Si:H (Refs. 24, 40, and 41) and attributed to structural relaxation. This provides another indication of a minimally disordered structure in the GD material.

Information on the state of disorder of the amorphous network can also be inferred from SAXS analysis. The diffuse scattering intensity from pure a-Si is $5.0 \pm 0.9\ e/a$, in the as-prepared state (Fig. 4).[14] Since the structures of the as-implanted a-Si and MH sample are expected to be comparable in terms of static disorder, the difference in their diffuse SAXS can arise only from a difference in the Laue monotonic scattering due to H alloying. Assuming a random distribution of H atoms, the expected Laue scattering from Eq. (5) for the MH sample is $3.3-4.4\ e/a$, smaller than the experimental difference $(13.7 \pm 0.6)_{\mathrm{MH}} - (5.0 \pm 0.9)_{\mathrm{unrelax}\ a\text{-}\mathrm{Si}} = 8.7 \pm 1.1\ e/a$. A first possible source of the deviation is the presence of vacancy defects (monovacancies or divacancies), likely related to H, which would increase the Laue scattering [Eq. (6)].[37] Consistent with this hypothesis are the H effusion experiments,[25] which indicated a relatively high density of vacancy-related defects in association with highly hydrogenated regions (i.e., >15 at. %) of an implanted a-Si sample. In addition, the presence of short-range H clusters (<0.5 nm) is presumed. As discussed in Sec. IV B, polyhydrides and monohydride groups will contribute more effectively to the Laue scattering than a random distribution of H atoms.

A direct comparison between the GD sample and pure a-Si of similar disorder is not possible. It is conceivable, though, that the contribution of the static disorder is close to the value measured in fully relaxed a-Si ($\sim 3.0\ e/a$).[20] Then, the expected Laue contribution of $4.3-5.8\ e/a$ for the GD sample would adequately account for the observed increase in the diffuse intensity relative to a relaxed a-Si network: $(7.0 \pm 0.6)_{\mathrm{GD}} - (3.0 \pm 0.9)_{\mathrm{relax}\ a\text{-}\mathrm{Si}} = 4. \pm 1.1\ e/a$. The agreement with the expected Laue scattering may imply a relatively modest short-range alloy clustering.

Finally, we turn to the difference in the experimental diffuse scattering between the MH and GD samples, which is almost a factor of 2 (Fig. 4). Based on the above discussion, we conclude that this difference derives primarily from a higher degree of H clustering on the atomic scale, not visible by IR absorption,[28] and/or a larger amount of vacancylike defects related to H in the implantanted material with respect to the GD sample. Second, the MH and the GD samples are characterized by a highly and a minimally disordered network, respectively. This introduces an additional difference, which is expected not to exceed $\sim 2\ e/a$, in the diffuse scattering intensity.

B. Thermal instability of the alloy structures

1. Implanted a-Si(H)

The observation of a thermal instability of the alloy structure of hydrogenated a-Si made by ion implantation and containing 11–12 at. % H confirms our earlier conclusions in relation to the effects of H concentration on the network

structure.[20,21] The investigation of hydrogenated layers containing 20 and 4 at. % as maximum [H] indicated the latter value to be the threshold for structural instability of the alloy. We proposed that only a limited concentration of H atoms (3–4 at. %) can be incorporated into the amorphous network in configurations that upon annealing remain dissolved in the matrix as Si-H bonds. The presently investigated sample contains H in excess of this limit, and has therefore an unstable structure, prone to inhomogeneity formation. Nanoscale H complexes are attributed to a process of H_2 formation followed by a coalescence of H_2 bubbles. The clustering process upon annealing is described in detail in Ref. 20.

More informative in the context of this paper is the comparison of the present SAXS data with results from the implanted sample containing 20 at. % H (HH sample),[20] since it throws light on the dependence of the precipitation on H concentration (Fig. 6). The precipitation phenomenon is quite similar for the MH and HH samples, both in volume fraction and in average size, up to about 400 °C. The volume fraction of the inhomogeneities diverges for the MH and HH samples after annealing treatments above 400 °C. Although the initial H concentration is less uniform in the HH sample than in the MH sample (Sec. III B), the volume content of the bubbles becomes considerably larger in the former sample. This provides evidence of a direct correlation between the amount of excess hydrogen (i.e., H concentration that exceeds the solubility) and the degree of precipitation. Since the *local* H concentration (i.e., peak regions) is a factor of 2 larger in the HH sample than in the MH sample, there is a greater supply of H in the H peaks of the HH sample to continue the growth of the inhomogeneities and thereby increase their volume content. Present results therefore demonstrate that the amount of H precipitation increases superlinearly with the excess hydrogen.

In the MH sample, the volume fraction appears to saturate and then decrease, while the bubble size monotonically increases [Fig. 6(b)]. The saturation of the volume fraction is consistent with a process of ripening of the H complexes upon annealing. Its decrease for $T>400$ °C is explained by the partial H out-diffusion, known to occur in the implanted sample in this temperature regime.[20] Hydrogen atoms from small H complexes can either diffuse out from the sample or contribute to the growth of bigger complexes.

2. PECVD *a*-Si:H

The most striking outcome of our SAXS data is that the structural modifications upon thermal treatment of the device-quality *a*-Si:H are qualitatively similar to those in the H-implanted *a*-Si. In other words, the nucleation of low-density defects shows that the structure of the device-quality *a*-Si:H is thermally unstable, as is the structure of implanted material containing [H] in excess of the solubility limit. There is an important consequence of this result. The existence of a stable alloy structure, i.e., H-implanted *a*-Si containing H up to 4 at. %,[20,21] suggests that 11 at. % H in PECVD *a*-Si:H is above the solubility limit, at least in the 400–450 °C temperature range. Moreover, this result points to a general behavior in the structural evolution of hydrogenated *a*-Si, independent of the preparation method of the samples, as already indicated by several experiments.[19,25,42]

In the following section we give a more detailed interpretation of the alloy instability of the device-quality *a*-Si:H and its implications for the modifications of the network disorder.

C. Nature of the alloy instability in device-quality *a*-Si:H

It is a well-known fact that annealing of device-quality *a*-Si:H at temperatures higher than 300–400 °C leads to an increase of the defect density, consistent with the release of H from the bonding sites.[43,44] The present investigation sheds more light on the correlation between the formation and growth of H complexes in the alloy and the change of the defect state of *a*-Si.

Based on the analysis in Sec. IV C, we concluded that the smaller-angle scattering, observed in the as-deposited GD sample, is due to both surface roughness and larger-scale bulk features.[45] Thus, in the initial state, the structure of the film is homogeneous on the nanoscale and may contain a very small amount of residual columnarlike structure. These features possibly consist of elongated lower-density regions that may be the precursors of a columnar growth. They should not, however, be thought of as a continuous pathway for H diffusion, for previous H evolution measurements have demonstrated a compact structure in device-quality *a*-Si:H in which H transport is diffusive.[46,47] In addition, the very low volume fraction of inhomogeneities derived from SAXS and the good electrical properties of the investigated film[26] exclude the hypothesis of correlated low-density regions. In agreement with this interpretation are earlier small-angle neutron-scattering studies[4] that found evidence for the presence of uncorrelated columnarlike hydrogenated regions in high-density material. The authors suggested that these features were consistent with linear or planar H complexes in the range of 6–12 nm. It is therefore possible that the residual columnar structures observed in the present GD sample are extended regions of enhanced H clustering.

Heating above 300 °C induces long-range hydrogen diffusion. Consequently, more H can accumulate in the extended hydrogenated regions, thereby increasing the density contrast associated with these features. A change in this contrast or an increase in the f of the larger-scale objects could produce the observed increase of the SAXS intensity upon annealing in the region $q \leqslant 1$ nm^{-1}, as seen by the increase of the Porod constant A (Table II and Sec. IV C). We implicitly assume in our model that annealing does not alter the surface roughness, at least on the scale of interest for SAXS. In concomitance with this process of accumulation of H in the columnarlike regions, a modification, on the atomic scale, of the structure takes place during annealing. In a first stage ($300<T<400$ °C), a part of the H atoms leaving the matrix moves to more clustered configurations, as deduced by the increase of the diffuse scattering (Fig. 4). Since the bond-angle distortion is not appreciably affected (Fig. 2), it is possible that the H in clustered configurations is mostly involved in this process. At $T \geqslant 400$ °C more hydrogen can be released, also those atoms bound to Si in more stable configurations. This leads to an increase of the overall state of disorder and thereby to an increase of the bond-angle distortion (Fig. 2). Hydrogen nanoclusters appear in the high-density bulk. The monotonic reduction with annealing tem-

perature of the average radius of the inhomogeneities, deduced from the analysis of the SAXS signals (Table II), arises from averaging the original larger-scale features with an increasing number of smaller-sized inhomogeneities (Sec. IV A).

At first sight, it appears difficult to reconcile a preferential release of H from the less tightly bound configurations with the increase of hydrogen clustering upon annealing in the 300–400 °C range. However, this can be explained by assuming that these processes predominantly involve the clustered phase. During annealing, H complexes with a radius smaller than a critical size tend to dissolve, while those with a larger critical radius grow, finally to a size that can be directly detected by SAXS.

We note that the present interpretation of the results can be considered consistent with the so-called H-deficit model.[48] It has been suggested[48] that two types of unhydrogenated sites exist in *a*-Si. The first type consists of configurations that are less effectively passivated by H probably the ones that bind H in the clustered phase. The second type is related to defects that bind H more strongly (e.g., dangling bonds). Likewise, present results suggest that hydrogen first leaves the sites that less effectively contribute to the release of the network disorder ($T<400$ °C), and later those defects that, if unhydrogenated, produce an abrupt rise in the state of disorder.

D. On the comparison of H-implanted *a*-Si and PECVD *a*-Si:H

Despite the qualitative resemblance of the structural evolution in the GD and MH samples, the magnitude of the H nanoclustering differs considerably in the two cases. The maximal volume fraction of the detected inhomogeneities for the *a*-Si:H remains a factor of 3 lower than that for the implanted material (Fig. 6). Considering the similar initial H content, this observation leads us to a discussion of the role of the initial defect state in the degree of H precipitation.

The overall state of disorder is drastically different in the two cases (Sec. V A). The implanted material is prepared by a highly nonequilibrium process, which makes the freezing in of a large concentration of defects possible.[15,16] Radiation damage induced by ion-implantation produces vacancylike defects[49] and may enhance H clustering on the atomic scale. It is possible that either vacancies, stabilized by the presence of H at their surface,[50] are a suitable site for the nucleation of H_2 bubbles, or that a more pronounced H clustered phase leads to a higher fraction of nanoscale H-rich defects in the implanted sample.

The *a*-Si:H film, on the contrary, is deposited under optimal conditions, at a low growth rate, which enables equilibration reactions to take place in the structure.[51] During growth, hydrogen can diffuse into the film and redistribute between bonding sites,[52] leading to a structure with low disorder and relatively modest alloy clustering.

A second difference is the temperature regime for the alloy instability. Nanoscale H complexes appear (i.e., volume fractions ~0.1 at. %) in the implanted material after heating above 250 °C, while temperatures above 350 °C are needed in the *a*-Si:H sample. This is readily explained by the preparation temperature of the materials. The initial temperature of the implanted material can be considered to be room temperature,[53] while the deposited film was grown at 250 °C.

Residual extended hydrogenated regions are present in the as-prepared state of the device-quality *a*-Si:H, whereas they are absent in the implanted material. This strongly suggests that these low-density regions are caused by the deposition process.

In the case of the H-implanted *a*-Si, we observe a gradual enlargement of the inhomogeneities with temperature [Fig. 6(b)]. Unfortunately, for the *a*-Si:H film, the presence of a smaller-angle scattering in the SAXS signal partially conceals the evolution of the nanoscale structure. It is therefore not possible to derive the size of the formed nanoscale particles, although the fits suggest a predominant component of inhomogeneities with a size similar to that of the MH sample (Sec. IV A).

VI. CONCLUSIONS

In this work, we have systematically investigated the thermal evolution of hydrogen-implanted *a*-Si, made by ion amorphization of crystalline Si, and a device-quality PECVD *a*-Si:H film. The atomic and nanoscale structure as well as the state of disorder have been characterized by small-angle x-ray scattering and Raman spectroscopy. The materials contain a similar initial H concentration (~11 at. %) and are both homogeneous on the nanoscale in the as-prepared state.

In hydrogenated *a*-Si made by implantation the thermal instability of the network structure occurs when the H concentration is above the solubility limit (3–4 at. %).[20,21] The *a*-Si(H) sample studied in this work contains 12 ± 1 at. % H and thus exhibits an unstable network structure. Comparison of the thermal evolution of the H nanoclusters in the present sample with one containing 20 at. % H demonstrates a direct correlation between the amount of H precipitation upon annealing and the concentration of H exceeding solubility. Results show that the volume content of the H complexes increases superlinearly with the excess H.

The evolution upon annealing of the alloy structure of device-quality PECVD *a*-Si:H bears qualitative resemblance to that of H-implanted *a*-Si with an H concentration exceeding the solubility limit. This demonstrates that device-quality *a*-Si:H with 11 at. % H does not have a stable network structure. Results for *a*-Si:H are not as complete as those for hydrogen-implanted material, mostly because it is unclear how a variation of the H concentration through a change in the plasma conditions influences the structure. For instance, a large decrease in H content would deteriorate the structural (and electronic) properties of PECVD material, since films would have to be deposited under conditions far from the optimum. We realize that it is not yet possible to make a conclusive and quantitative statement on the solubility limit of H in the case of PECVD *a*-Si:H, but, in light of the present results, we do propose that it exists.

Finally, the volume fraction of H nanoclusters is much smaller in *a*-Si:H than that in the implanted material, suggesting a correlation between the initial defect structure and (the amount of) H nanoclustering. Together with the solubility limit for *a*-Si:H, results would imply a larger H solubility in the PECVD *a*-Si:H than in the amorphized material.

ACKNOWLEDGMENTS

We are sincerely grateful to W. M. Arnold Bik for ERD measurements. In the preliminary phase of this work we benefited from discussions with P. A. Stolk. This work was financially supported by the Netherlands Organization for Scientific Research (NWO). The work at the CSM was supported by the National Renewable Energy Laboratory under Subcontract No. XAN-4-13318-04. Work at the UdM was supported by the Natural Sciences and Engineering Research Council of Canada (NSERC) and the Fonds pour la Formation des Chercheurs et de l'Aide a la Recherche (FCAR).

---

*Present address: Research Institute for Materials, University of Nijmegen, P.O. Box 9010, 6500 GL Nijmegen, The Netherlands.

†Permanent address: Energieonderzoek Centrum Nederland (ECN), P.O. Box 1, 1755 ZG Petten, The Netherlands.

[1] G. Lucovsky, R. J. Nemanich, and J. C. Knights, Phys. Rev. B **19**, 2064 (1979).

[2] J. A. Reimer, R. Vaughan, and J. C. Knights, Solid State Commun. **37**, 161 (1981).

[3] J. Baum, K. K. Gleason, A. Pines, A. N. Garroway, and J. A. Reimer, Phys. Rev. Lett. **56**, 1377 (1986).

[4] R. Bellisant, in *Amorphous Silicon and Related Materials*, edited by H. Fritzsche (World Scientific, Singapore, 1988), p. 93.

[5] C. A. Guy, A. C. Wright, R. N. Sinclair, R. J. Stewart, and F. Jansen, J. Non-Cryst. Solids **196**, 260 (1996).

[6] D. L. Williamson, in *Amorphous Silicon Technology—1995*, edited by M. Hack, A. Madan, M. Powell, and A. Matsuda, MRS Symposia Proceedings No. 377 (Materials Research Society, Pittsburgh, 1995), p. 251.

[7] J. A. Reimer, R. Vaughan, and J. C. Knights, Phys. Rev. B **24**, 3360 (1981).

[8] J. Shinar, H. J. Hia, R. Shinar, Y. Chen, and D. L. Williamson, Phys. Rev. B **50**, 7358 (1994).

[9] R. S. Crandall, X. Liu, and E. Iwaniczko, J. Non Cryst. Solids **227-230**, 23 (1998).

[10] W. B. Jackson, P. V. Santos, and T. C. Tsai, Phys. Rev. B **47**, 9993 (1993).

[11] I. An, Y. M. Li, C. R. Wronsky, and R. W. Collins, Phys. Rev. B **48**, 4464 (1993).

[12] N. H. Nickel and W. B. Jackson, Phys. Rev. B **51**, 4872 (1995).

[13] J. P. Conde, M. Gonçalves, P. Brogueira, V. Schotten, and V. Chu, Phys. Rev. B **53**, 1886 (1996).

[14] D. L. Williamson, S. Roorda, M. Chicoine, R. Tabti, P. A. Stolk, S. Acco, and F. W. Saris, Appl. Phys. Lett. **67**, 226 (1995).

[15] P. A. Stolk, F. W. Saris, A. J. M. Berntsen, W. F. van der Weg, L. T. Sealy, R. C. Barklie, G. Krötz, and G. Müller, J. Appl. Phys. **75**, 7266 (1994).

[16] S. Roorda, W. C. Sinke, J. M. Poate, D. C. Jacobson, S. Dierker, B. S. Dennis, D. J. Eaglesham, F. Spaepen, and P. Fuoss, Phys. Rev. B **44**, 3702 (1991).

[17] W. G. Spitzer, G. K. Hubler, and T. A. Kennedy, Nucl. Instrum. Methods Phys. Res. **209/210**, 309 (1983); B. Rakvin, B. Pivac, and R. Reitano, J. Appl. Phys. **81**, 3453 (1997).

[18] K. F. Heidemann, M. Grüner, and E. te Kaat, Radiat. Eff. **82**, 103 (1984).

[19] K. Böhringer, X. H. Liu, and S. Kalbitzer, J. Phys. C **16**, L1187 (1983).

[20] S. Acco, D. L. Williamson, P. A. Stolk, F. W. Saris, M. J. van der Boogaard, W. C. Sinke, W. F. van der Weg, S. Roorda, and P. C. Zalm, Phys. Rev. B **53**, 4415 (1996).

[21] K. Jones, D. L. Williamson, S. Acco, and M. M. Al-Jassim, in *Proceedings Microscopy and Microanalysis*, edited by G. W. Bailey (San Francisco Press, San Francisco, 1996), p. 972.

[22] P. V. Santos, N. M. Johnson, and R. A. Street, Phys. Rev. Lett. **67**, 2686 (1991).

[23] Z. Yiping, Z. Dianlin, K. Guanglin, P. Guangqin, and L. Xianbo, Phys. Rev. Lett. **74**, 558 (1995).

[24] W. C. Sinke, T. Warabisako, M. Miyao, T. Tokuyama, S. Roorda, and F. W. Saris, J. Non-Cryst. Solids **99**, 308 (1988).

[25] S. Acco, W. Beyer, E. E. van Faassen, and W. F. van der Weg, J. Appl. Phys. **82**, 2862 (1997).

[26] W. G. J. H. M. van Sark, J. Bezemer, and W. F. van der Weg, J. Mater. Res. **13**, 45 (1998).

[27] D. Beeman, R. Tsu, and M. F. Thorpe, Phys. Rev. B **32**, 874 (1985).

[28] S. Acco, Ph.D. thesis, Utrecht University, 1997.

[29] H. Shanks, C. J. Fang, L. Ley, M. Cardona, F. J. Demond, and S. Kalbitzer, Phys. Status Solidi **100**, 43 (1980).

[30] S. J. Jones, A. B. Shwartzlander, Y. Chen, and D. L. Williamson, in *Amorphous Silicon Technology—1993*, edited by E. Shiff, M. J. Thompson, A. Madan, K. Tanaka, and P. G. LeComber, MRS Symposia Proceedings No. 297 (Materials Research Society, Pittsburgh, 1993), p. 1049.

[31] A. Guinier and G. Fournet, *Small-Angle Scattering of X-rays* (Wiley, New York, 1955).

[32] N. W. Ashcroft and J. Lekner, Phys. Rev. **145**, 83 (1966); R. Triolo, E. Caponetti, and S. Spooner, Phys. Rev. B **39**, 4588 (1989).

[33] V. Gerold, in *Small-Angle X-ray Scattering*, edited by H. Brumberger (Gordon and Breach, New York, 1967).

[34] Y. J. Chabal and C. K. N. Patel, Phys. Rev. Lett. **53**, 210 (1984).

[35] H.-G. Haubold and D. Martinsen, J. Appl. Crystallogr. **11**, 592 (1978).

[36] S. Chattopadhay, S. N. Sharma, R. Banerjee, D. M. Bushari, S. T. Kshirgasar, Y. Chen, and D. L. Williamson, J. Appl. Phys. **76**, 5208 (1994).

[37] R. Lutz and L. J. Lewis, Phys. Rev. B **47**, 9886 (1993).

[38] S. Muramatsu, S. Matsubara, T. Watanabe, T. Shimada, T. Kamiyana, K. Suzuki, and A. Matsuda, Jpn. J. Appl. Phys., Part 2 **30**, L2006 (1991).

[39] D. L. Williamson (unpublished).

[40] A. J. M. Berntsen, Ph.D. thesis, University Utrecht, 1993.

[41] Y. Hiroyama, R. Suzuki, Y. Hirano, F. Sato, and T. Motooka, Jpn. J. Appl. Phys., Part 1 **34**, 5515 (1995).

[42] K. Böhringer, H. Mannsperger, and S. Kalbitzer, Nucl. Instrum. Methods Phys. Res. B **7/8**, 299 (1985).

[43] K. Biegelsen, R. A. Street, C. C. Tsai, and J. K. Knights, Phys. Rev. B **20**, 4839 (1979).

[44] K. Zellama, L. Chahed, P. Sladek, M. L. Theye, J. H. von Bardeleben, and P. Roca i Cabarrocas, Phys. Rev. B **53**, 3804 (1996).

[45] Under the assumption that a smaller-angle scattering arises solely from surface-related defects, it becomes difficult to explain the process of a sudden nucleation of relatively large nanoparticles ($\langle R\rangle \sim 1.5$ nm), which appear to shrink in size with increasing temperature (Table II). This interpretation goes against the step-

by-step increase of H nanoclustering and disorder deduced from SAXS and Raman experiments.

[46] W. Beyer and H. Wagner, J. Appl. Phys. **53**, 8745 (1982).
[47] W. B. Jackson, N. H. Nickel, N. M. Johnson, F. Pardo, and P. V. Santos, in *Amorphous Silicon Technology—1994*, edited by E. A. Schiff *et al.*, MRS Symposia Proceedings No. 336 (Materials Research Society, Pittsburgh, 1994), p. 311.
[48] S. Zafar and E. A. Shiff, Phys. Rev. Lett. **66**, 1493 (1991).
[49] B. Nielsen, O. W. Holland, T. C. Leung, and K. J. Lynn, J. Appl. Phys. **74**, 1636 (1993).
[50] B. Turtle and J. B. Adams, Phys. Rev. B **53**, 16 265 (1996).
[51] D. V. Tsu, B. S. Chao, S. R. Ovhinsky, S. Guha, and J. Yang, Appl. Phys. Lett. **71**, 1317 (1997).
[52] R. A. Street, Phys. Rev. B **43**, 2454 (1991).
[53] As mentioned in Sec. II, all samples were implanted at liquid-nitrogen temperature (LNT) ($\sim$77 K). It has been found [S. Coffa, F. Priolo, and A. Battaglia, Phys. Rev. Lett. **70**, 3756 (1993)] that at LNT a different distribution of defects exists in ion-implanted a-Si, than at room temperature (RT), which partly annihilates when the sample warms up to RT. Since measurements are performed at RT, the defect population present in a-Si(H) is that characteristic of that very temperature. We can therefore consider RT as the ''initial'' temperature for the implanted samples.